

Synchronization of fluctuating delay-coupled chaotic networks

Manuel Jiménez,¹ Javier Rodríguez-Laguna,¹ Otti D’Huys,² Javier de la Rubia,¹ and Elka Korutcheva^{1,3}

¹*Departamento de Física Fundamental, UNED, Spain*

²*Department of Mathematics, Aston University, B7 4ET Birmingham, United Kingdom*

³*G. Nadjakov Inst. Solid State Physics, Bulgarian Academy of Sciences, 1784, Sofia, Bulgaria*

(Dated: May 22, 2019)

We study the synchronization of chaotic units connected through time-delayed fluctuating interactions. We focus on small-world networks of Bernoulli and Logistic units with a fixed chiral backbone. Comparing the synchronization properties of static and fluctuating networks, we find that random network alternations can enhance the synchronizability. Synchronized states appear to be maximally stable when fluctuations are much faster than the time-delay, even when the instantaneous state of the network does not allow synchronization. This enhancing effect disappears for very slow fluctuations. For fluctuation time scales of the order of the time-delay, a desynchronizing resonance is reported. Moreover, we observe characteristic oscillations, with a periodicity related to the coupling delay, as the system approaches or drifts away from the synchronized state.

I. INTRODUCTION

Cooperative behavior of chaotic systems in interaction can lead to the emergence of partial and local synchronization [1]. An interesting problem in this context is the stability of the synchronized state, which is ruled by the topology of the interaction [2, 3]. In most settings, the coupling terms carry a finite time-delay due to the finite velocity of transmission of information. Yet, even for infinitely large time-delay the units can achieve zero-lag synchronization [4]. The paradigmatic time-delayed coupled systems capable of chaos synchronization are semiconductor lasers [5–8], with interesting applications in secure communication [9, 10]. The phenomenon might have relevance as well in neuroscience [11, 12].

A better understanding of chaos synchronization can be gained by studying simple chaotic systems, such as Bernoulli maps under single [13] or multiple [14] time-delays, for which the conditions for a stable synchronized state can be obtained analytically. These studies generally perform a stability analysis of the synchronized state on a fixed interaction network. Additionally, a general formalism has been developed for ensembles of static random interaction networks [15].

Currently, there is an increasing interest in studying networks as time-varying entities [16]. In fact, network fluctuations are essential features of some systems such as, for instance, interacting neurons, where synaptic plasticity continuously changes the topology [17]. It is interesting then to inquire how does a fluctuating network affect synchronization stability [18]. Recently, there has been a number of studies concerning synchronization on time-varying contact networks, where the topology changes due to the random motion of the agents, and the couplings are instantaneous. Most of them consider diffusive coupling of moving oscillators [19, 20], but also chaotic units [21, 22]. This problem has also been tackled for genetic oscillators moving on lattices [23, 24]. In this paper we study the synchronization properties of chaotic maps interacting on random small-world directed net-

works whose topology fluctuates in time and whose links bear a large time-delay. There has been a very recent work concerning the case of coupled chaotic maps interacting with small time-delays comparable to the time scale of network switching [25]. Our work builds on the previous studies by exploring synchronization stability on the full range of possible scalings between the time-delay and the network switching time scale.

We consider an interaction network of coupled chaotic maps with a single coupling delay, T_d . The networks fluctuates with a characteristic time-scale T_n . These network fluctuations are random, and not adaptive, i.e., the network evolution is not linked to the state in any way. If $T_n \gg T_d$, i.e., the slow network regime, the dynamics always have enough time to adapt to the current network. Therefore, if the network acquires a desynchronizing configuration, it will lose synchronization. Resynchronization, although possible in principle, is unlikely, for the chaotic maps that we consider. Thus, we may regard the long term dynamics as desynchronized whenever the probability of reaching a non-synchronizing network is finite. The case where T_n is comparable to T_d or smaller is more involved. Indeed, the system will spend time both in synchronizing and de-synchronizing networks. When the network reaches a de-synchronizing configuration, it will start to escape the synchronization manifold. But, if T_n is not large enough, there is a probability of returning to a synchronizing configuration before a certain *irreversibility line* is crossed. Thus, the system may stay synchronized. Indeed, our results will prove stronger: when $T_n \ll T_d$, in the fast fluctuations regime, synchronization becomes significantly more stable. This is in qualitative agreement with the fast switching approximation [26], which states that synchronization is possible for fast fluctuating networks and diffusive coupling if the time averaged graph laplacian synchronizes.

This paper is organized as follows. Section II defines our time-delayed dynamical system, and reviews the basic framework for its study. In section III we study in detail the synchronizability in the case of (static) small-world networks. Then, we define our fluctuating net-

works, the observables to be employed, and discuss the numerical results in detail in IV. The last section is devoted to the conclusions and further work.

II. SYNCHRONIZATION OF DELAYED CHAOTIC NETWORKS

Let us consider N classical units, characterized by a single degree of freedom $u_i(t)$, $i \in \{1, \dots, N\}$ and time $t \in \mathbb{N}$, whose evolution is given by:

$$u_i(t+1) = (1-\epsilon)f(u_i(t)) + \epsilon \sum_j G_{ij}(t)f(u_j(t-T_d)), \quad (1)$$

where $\epsilon \in [0, 1]$ is a real parameter which measures the strength of the interaction, T_d is the coupling delay and $f: [0, 1] \mapsto [0, 1]$ is a chaotic map. We consider the Bernoulli map, modeled as

$$f(x) = ax \mod 1, \quad (2)$$

with $a \in \mathbb{R}^+$, and the Logistic map, given by

$$f(x) = rx(1-x), \quad (3)$$

with $r \in \mathbb{R}^+$. The network structure is described the adjacency matrix G . To ensure the *existence* within a synchronized dynamical state, the adjacency matrix is subject to a unit row-sum condition (also known as stochasticity condition),

$$\sum_j G_{ij}(t) = 1, \quad (4)$$

for all i and all times t . Nonetheless, this does not inform us about the stability of such synchronized state.

As a measure of the (zero-lag) synchronization in the network, we have chosen the logarithm of the spatial deviation over the network nodes. Let us explain in detail the meaning of this observable. Consider the spatial average of the unit states for a given time as

$$\mu(t) \equiv \frac{1}{N} \sum_{i=1}^N u_i(t), \quad (5)$$

and the corresponding spatial standard deviation as

$$\sigma \equiv \sqrt{\frac{1}{N} \sum_{i=1}^N (u_i - \mu)^2}. \quad (6)$$

Then, the *synchronization level* is defined as

$$\mathcal{S} \equiv -\ln(\sigma). \quad (7)$$

A perfectly synchronized state would have $\mathcal{S} \rightarrow +\infty$, but in practice this value is bounded by the machine precision. In our calculations, using double precision floating point numbers, this value corresponds approximately to $\mathcal{S} \sim 35$, which implies a deviation of order $\sigma \sim \exp[-35] \sim 10^{-15}$. On the other extreme, in a desynchronized state each unit behaves independently and $\mathcal{S} = O(1)$. In our experiments, the minimal value of \mathcal{S} is close to 1.95, which is close to the mean deviation for a uniform distribution on $[0, 1]$: $-\ln \sigma = -\ln(12)/2 = 1.24$.

We initialize the network close the synchronized state: all units evolve in unison for T_d time steps, and we apply at $t = 0$ a random point-like perturbation $\xi = A \cdot \mathbf{r}$, with $A = 10^{-10}$ and \mathbf{r} is a vector of random numbers drawn uniformly from $[0, 1]$. Thus, the synchronization level at $t = 0$ is always around 25, instead of the machine precision value of 35. We will denote by $\langle \cdot \rangle$ the *realization average* over such initial conditions. Our most relevant observable, therefore, will be $\langle \mathcal{S}(t) \rangle$.

We define a *synchronization Lyapunov exponent* (SLE) as the average linear rate at which the synchronization level increases or decreases with time:

$$\langle \mathcal{S}(t) \rangle \sim \mathcal{S}_0 - \lambda t. \quad (8)$$

By this definition, λ is equivalent to the maximal Lyapunov exponent transverse to the synchronization manifold, given by the master stability function [2], which approximates the evolution of a perturbation from the synchronized state $\sigma \sim (u_i - \mu) \propto e^{\lambda t}$.

The stability of the synchronized state is related to the second largest eigenvalue of the adjacency matrix G . Let $\{\gamma_i\}_{i=1}^N$ be the eigenvalues of G sorted in descending order of their modulus, $|\gamma_1| \geq |\gamma_2| \geq \dots \geq |\gamma_N|$. Gerschgorin circle theorem [27] can be applied, showing that $|\gamma_i| \leq 1$, and the unit row sum guarantees that $|\gamma_1| = 1$, with eigenvector $[1, \dots, 1]$. Hence, a perturbation along this mode preserves synchronization as it affects every unit equally. The evolution of a perturbation away from the synchronization manifold will then evolve according the mode with second largest eigenvalue [2].

For a network of Bernoulli maps (Eq. (2)), assuming that $(a(1-\epsilon))^{T_d} \ll 1$ and $(a\epsilon|\gamma_2|)^{T_d} \ll 1$ hold, the SLE can be approximated by the following expression [10, 28].

$$\lambda \approx \frac{1}{T_d} \ln \left| \frac{a\epsilon\gamma_2}{1 - a(1-\epsilon)} \right| \quad (9)$$

Hence, the condition for a stable synchronization manifold reads:

$$\epsilon > \frac{a-1}{a\Delta}, \quad (10)$$

where $\Delta = 1 - |\gamma_2|$ is the *spectral gap* or *eigengap*.

For other chaotic maps, the stretch factor of the map $|f'(x)|$ is not constant, and the SLE is not analytically accessible. However, it has been shown that fluctuations

in the term $|f'(x)|$ along the chaotic trajectory result in a larger spectrum of Lyapunov exponents and thus in a smaller parameter region that sustains stable synchronization [29]. We will study synchronization stability on fluctuating networks of coupled Bernoulli maps in order to be able to compare with the analytical results for static networks. We will also study networks of Logistic maps in order to assess the generality of our results.

III. SYNCHRONIZATION OF SMALL-WORLD STATIC NETWORKS

We have studied the stability of the synchronization manifold on statistical ensembles of small world networks, which constitute a standard benchmark for network synchronization [18, 30–32]. Here, we will consider a family of Newman-Watts networks [33], similar to the standard small-world [34] but keeping the outside ring fixed, so that it is guaranteed that the network is always connected. We will refer generically to these networks as small world (SW).

To construct our networks, we consider a chiral 1D chain of N sites, where the only non-zero entries have the form $G_{i,i+1}$, with periodic boundary conditions. Then we add to the chiral backbone a number of $\langle pN \rangle$ of directed *shortcuts*, connecting random sites, with $p \in [0, 1]$. An example of such a SW network, with $N = 30$ and $p = 0.3$ is shown in Fig. 1 (top) for illustration.

A first requirement for complete synchronization is given by the GCD condition, which states that the number of possible synchronized subnetworks is equal to the Greatest Common Divisor (GCD) of the loop lengths of the network [13]. Hence, complete synchronization is only possible if the GCD of the lengths of all cycles in the network is unity. This is almost always the case for large enough networks with a finite number of shortcuts, as can be seen in Fig. 1 (bottom). When the GCD condition is met, the stability of the synchronization manifold is still determined by the eigengap, as stated in Eq. (10) for the specific case of Bernoulli maps.

The adjacency matrices G of directed networks are not hermitian, and their spectrum need not be real. Let us discuss the statistical properties of their spectra, in similarity to the studies of [32, 35]. Fig. 2 (top) shows the eigenvalues $\{\gamma_i\}$ on the complex plane for two SW networks, using $N = 500$ and $p = 1/5$ (left) and $1/2$ (right). Notice that, following Gerschgorin theorem, they are always contained within the unit circle. Except for the $\gamma_1 = 1$ eigenvalue, which is a consequence of the row-sum condition, the phases of the eigenvalues seem to be homogeneously distributed. Moreover, they seem to be contained within a ring, whose radius we would like to characterize.

An interesting approach to estimate the properties of the spectrum of random matrices describing SW networks was developed in [32], using a mean-field approach: write down the *average matrix*, whose entries are given

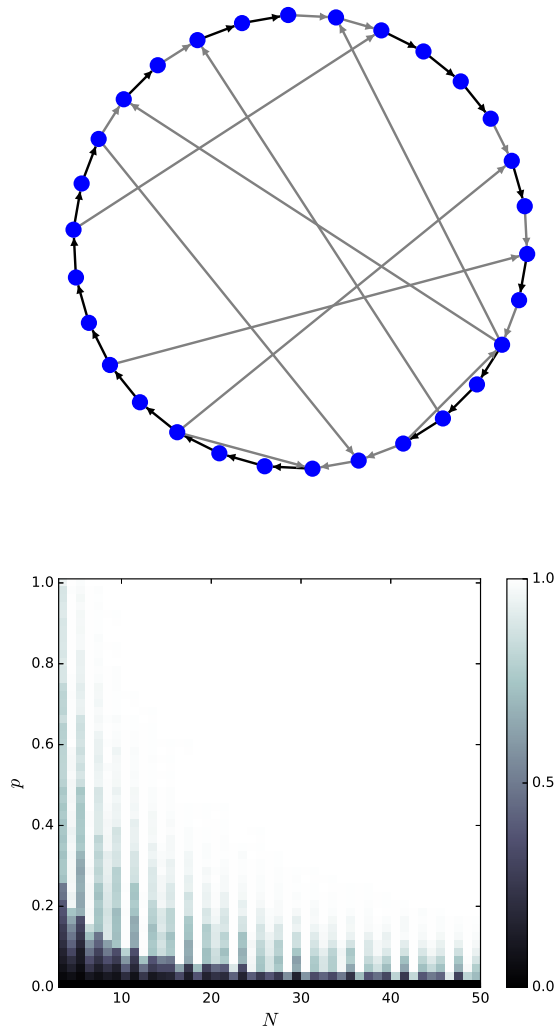


Figure 1: Top: Illustrating the directed networks used in our dynamical systems. In the example, a $N = 30$ network with a clockwise rotating backbone and $p = 0.3$, so the number of shortcuts is $N_s = 9$. The strength of each link is denoted by its color: black is 1 and gray is $1/2$. Notice that the sum of input links on any node is always 1, as imposed in Eq. (4). Bottom: Average fraction of the networks having $GCD = 1$ in the $N \times p$ space. For high enough number of units and shortcuts the probability of $GCD > 1$ is negligible.

by the average of the matrix entries. Due to translation invariance, the resulting matrix is a *circulant matrix*, whose spectrum can be found analytically. We have followed this approach in order to find the mean field spectrum of our SW networks. In the appendix A we show that the spectrum of this average matrix lies in the vicinity of a circumference of radius

$$|\gamma_m^{\text{MF}}| \approx \frac{1 - e^{-p}}{p}, \quad (11)$$

which appears marked in Fig. 2 (top) as *mean-field* line.

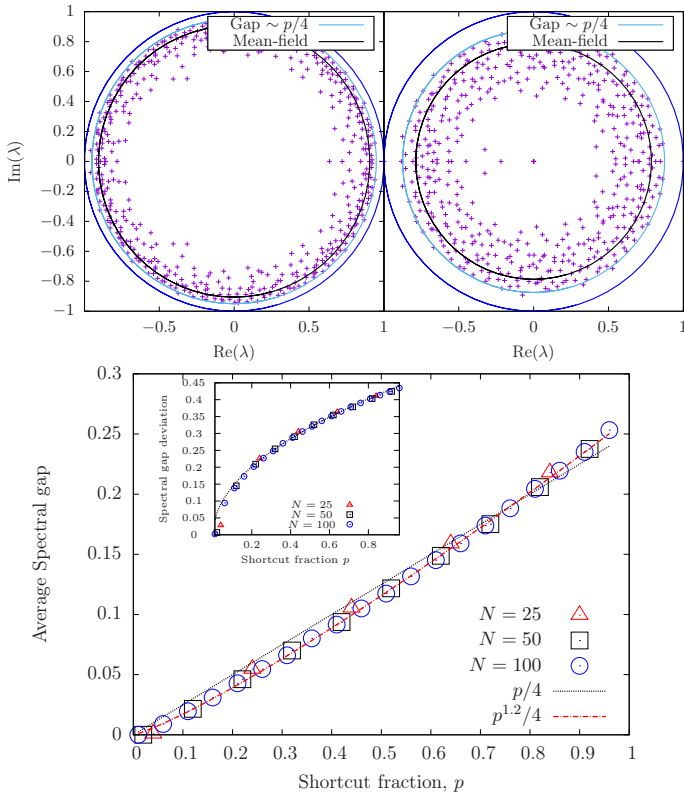


Figure 2: Top: Spectrum of the adjacency matrix of two SW networks, using $N = 500$, and $p = 1/5$ (left) and $1/2$ (right). Notice that most of the eigenvalues are contained within a ring, whose inner and outer radii are discussed in the text. Bottom: spectral gap for different values of N as a function of p of our SW networks, which grows approximately as $p/4$. A more accurate fit, with exponent 1.2 is also shown. Inset: Standard deviation of the gap scales as the square root of p .

Note that this mean-field theory does not provide an explanation for the ring structure of the spectrum. We have found numerically that the outer circumference has an approximate radius of $(1 - p/4)$, independent of N . Thus, our estimate for the gap is

$$\Delta \approx p/4. \quad (12)$$

The lower panel of Fig. 2 shows the numerical evidence for expression (12), plotting the average spectral gap as a function of p for different system sizes N . Interestingly, the inset shows that the standard deviation of the spectral gap among samples only grows like the square root of p , $\sigma_\Delta \sim p^{1/2}/2$.

Once the spectral properties of our networks have been elucidated we can proceed to study their dynamics. We have simulated the dynamical system Eq. (1) and obtained numerically the synchronization Lyapunov exponent (SLE) for 10^5 different SW networks with $N = 40$, $T_d = 100$, $\epsilon = 0.7$, two values of $p = 0.5$ and 0.8 , and two maps: Bernoulli, Eq. (2), and Logistic, Eq. (3). We have chosen the numerical values of the parameters

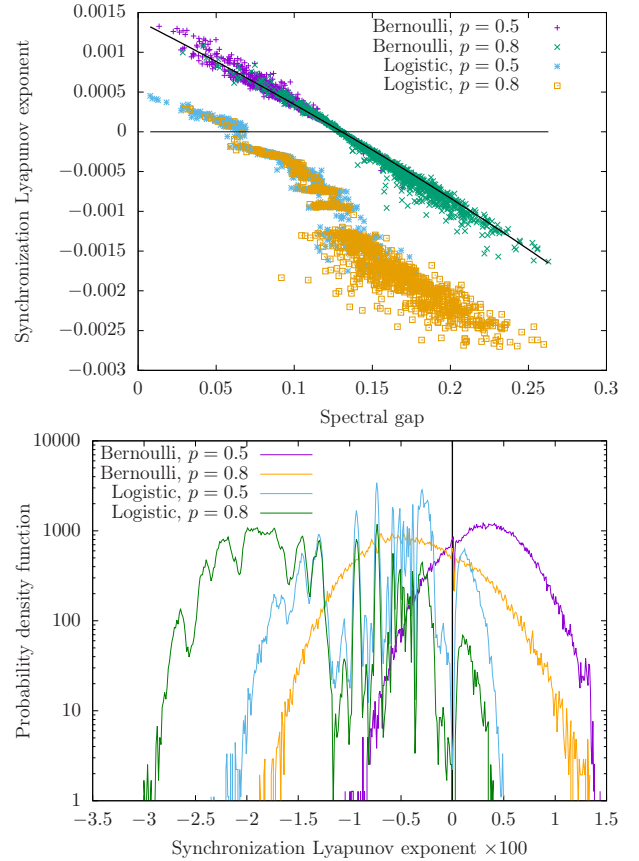


Figure 3: Measurement of the synchronization Lyapunov exponent (SLE) along with the spectral gap for 10^5 samples of two SW network ensembles with $N = 40$ sites, $\epsilon = 0.7$, and $p = 0.5$ and $p = 0.8$, for two different dynamical systems: Bernoulli and Logistic. Top: Relation between the SLE and the spectral gap. The black line corresponds to the theoretical expression Eq. (9) for coupled Bernoulli maps with long delays, and captures correctly the measured SLE, specially at values close to zero. For the Logistic maps, the correlation is still strong, but much more involved. Bottom: SLE histogram for the same four cases, in log-scale. Notice that, for Bernoulli we obtain an approximately Gaussian behavior, with non-zero skewness. For the Logistic case, the SLE are distributed in a much more complicated way. The vertical black bar marks the zero SLE, so on the left we have synchronization.

$a = 1.1$ and $r = 3.577$ so both maps have comparable Lyapunov exponents when considered in isolation, [41].

In Fig. 3 (top) we plot those values of the SLE vs the spectral gap of each network. In the Bernoulli case we find a nearly linear relationship, with a higher probability of synchronization (negative SLE) for $p = 0.8$. The Logistic case is more involved, but the negative correlation between both magnitudes is still clear. In general terms we can see that it synchronizes better.

Fig. 3 (bottom) shows the histogram of the SLE for Bernoulli and Logistic systems, using always $N = 40$, $T_d = 100$, $\epsilon = 0.7$ and two values of $p = 0.5$ and 0.8 . The black vertical bar marks the zero value: points on its left

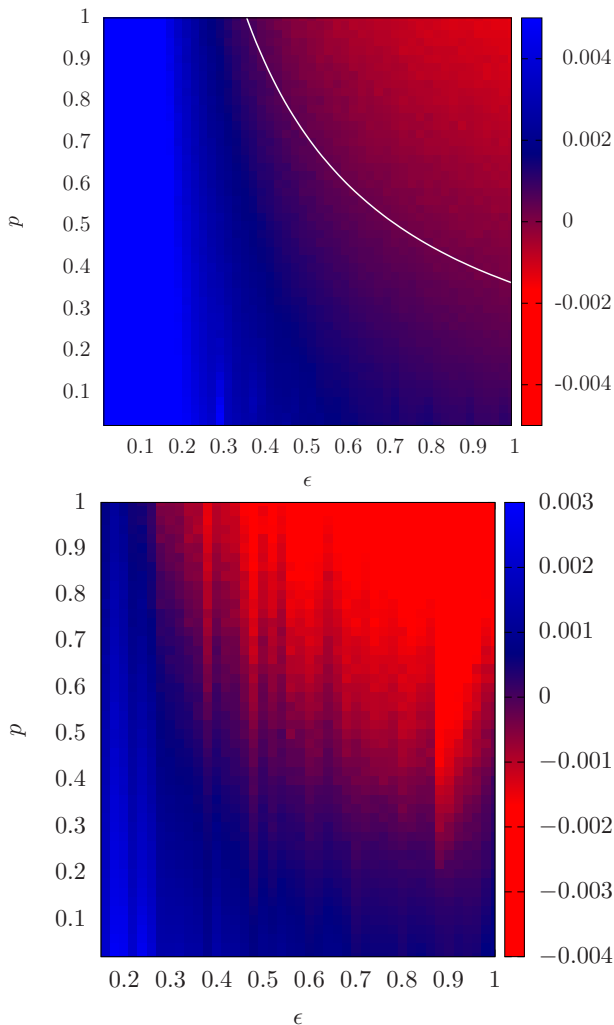


Figure 4: Average SLE for our SW networks as a function of both ϵ and p , using 100 samples for each point. Top: Bernoulli map. Bottom: Logistic map. The white line delimits the theoretical synchronization region, Eq. 10, for a static network of Bernoulli maps and eigengap $\Delta = p/4$.

correspond to networks in which the synchronized state is stable. The histograms for the Bernoulli case have a nearly Gaussian shape, but with finite skewness and kurtosis [36]. The histograms are much more involved for the Logistic case.

We have also performed a thorough exploration of the parameter space, ϵ and p , finding the average value of the SLE in Fig. 4 after 100 samples for each point, top for the Bernoulli map and bottom for the Logistic one. In both figures, red represents negative SLE, which allow for stable synchronization, while blue stands for positive values, which drive the system away from the synchronized state. The white line represents the theoretical synchronization line for networks of Bernoulli maps Eq. (10) for an eigenvalue gap of $\Delta = p/4$, and follows the zero average SLE accurately.

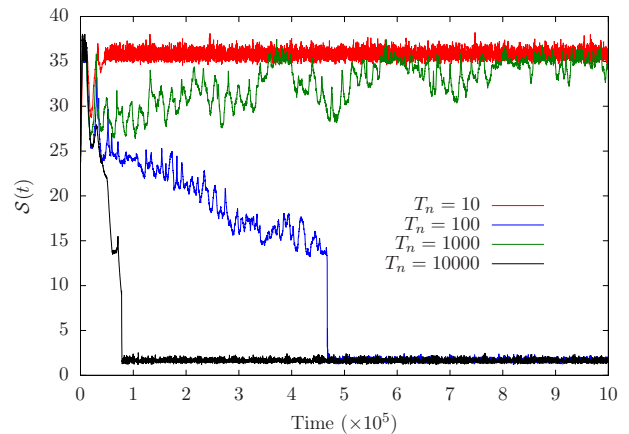


Figure 5: Synchronization level as a function of time for four histories of our dynamical system with $N = 40$, $p = 0.5$, $T_d = 100$ and $\epsilon = 0.7$ using different fluctuation times: $T_n = 10$, 10^2 , 10^3 and 10^4 . The units are Bernoulli maps.

IV. FLUCTUATING NETWORKS

Let us allow our networks to fluctuate, making G time-dependent with a network switching period T_n : the coupling topology will switch from the current network, G_{curr} , to a newly sampled G_{next} every T_n time steps. We sample from the ensemble of all SW graphs with fixed N and p defined in section III. We normalize each row by its sum so that the resulting networks verify the unit row-sum constraint Eq. (4) and the synchronized solution exists. The Bernoulli and Logistic map parameter values for a and r , respectively, are the same as in the preceding section III.

As a first attempt, we see in Fig. 5 a few \mathcal{S} time traces of fluctuating SW networks of Bernoulli maps with $N = 40$, $p = 1/2$, $\epsilon = 0.7$, and different fluctuation times: $T_n = 10$, 10^2 , 10^3 and 10^4 . Unless otherwise stated, we will always choose $T_d = 100$ for the time-delay. For $T_n = 10^4$, the synchronization level decays to its minimal value very fast, since the average SLE is positive, and full de-synchronization is irreversible. For $T_n = 1000$, we observe strong fluctuations in the state deviation, but an ultimate synchronization. For $T_n = 100$, when the fluctuation time-scale coincides with the delay, the system also desynchronizes, although more slowly. For $T_n = 10$, the system synchronizes fully quite fast.

Let us average the synchronization level for a large number of realizations, $N_s = 1000$. Fig. 6 shows the results for three different systems of coupled Bernoulli maps, showing only time steps which are multiples of $T_d = 100$. In Fig. 6 (top) we show the average synchronization for the same system as Fig. 5, in order to assess whether those results are generic. We see that for very short fluctuation time $T_n = 1$ or 10 , the system synchronizes quite fast. For $T_n = 50$ the synchronization level decays very slowly with time, and it decays much faster for $T_n = 100$. As we increase the fluctuation time scale,

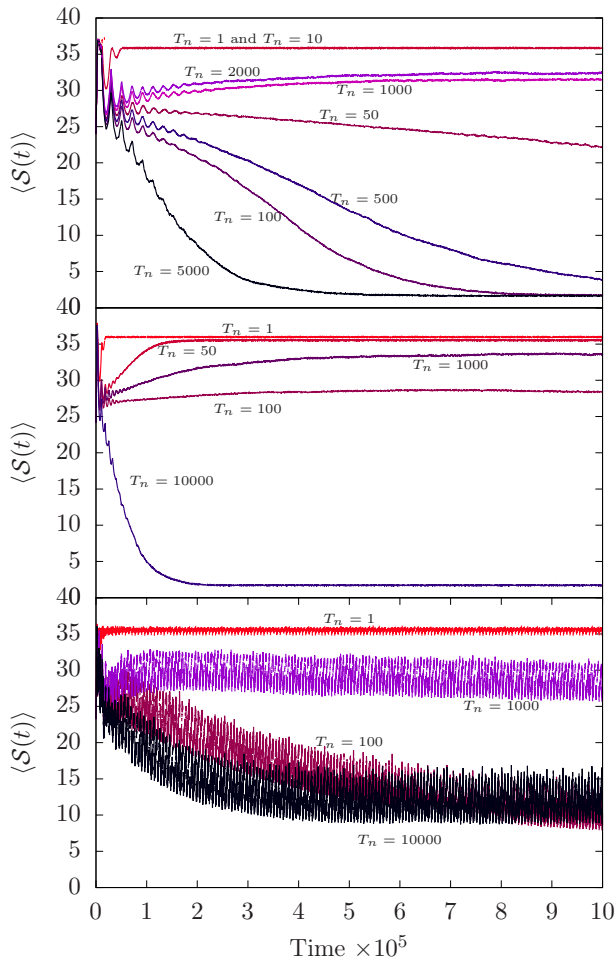


Figure 6: Realization average of the synchronization level, $\langle \mathcal{S}(t) \rangle$, Eq. (7), over $N_s = 1000$ samples, as a function of time for different systems. Top: Bernoulli system, $N = 40$, $p = 0.5$ and $\epsilon = 0.7$ (in average, non-synchronizing), for different values of T_n . Center: Bernoulli system with $N = 40$ sites, $p = 0.8$ and $\epsilon = 0.47$ (in average, synchronizing), for different values of T_n . Bottom: Logistic system, $N = 40$, $p = 0.5$ and $\epsilon = 0.4$ (in average, non-synchronizing). In all cases, $T_d = 100$, and we only show time steps which are multiples of 100.

for $T_n = 500$, the synchronization decay is again a bit slower, and for $T_n = 1000$ or 2000 we can see that the system does not seem to desynchronize, but stays at a lower level of synchronization. For even slower fluctuations, $T_n = 5000$, the system desynchronizes again quite fast. We should also remark the presence of oscillatory behavior for short times.

The lower panels of Fig. 6 explore different systems. The central one shows the case of a Bernoulli system over SW networks with $N = 40$, $p = 0.8$ and $\epsilon = 0.47$, a parameter choice for which the average SLE is negative, hence the system is synchronizing. The main difference that we can observe is that for $T_n = 100$ the system does not desynchronize, even though the asymptotic synchronization level is lower than for $T_n = 50$ and $T_n = 1000$.

However, for $T_n = 10000$ the system still desynchronizes. One may ask how is it possible that, if the system is in average synchronizing, the system desynchronizes in the long run for slow network fluctuations. The reason is that, for Bernoulli systems, desynchronization is *irreversible*. Once a certain \mathcal{S} threshold is crossed, the system will be too far away from the synchronization manifold and the subsequently sampled synchronizing networks will not take the system back to synchronization. The short time oscillations that we observed in the previous case are still present, but attenuated.

The lowest panel of Fig. 6 shows the average synchronization level for a Logistic system on fluctuating SW networks with $N = 40$, $p = 1/2$ and $\epsilon = 0.4$ (in average, non-synchronizing). Again, we observe that $T_n = 100$, coinciding with the time-delay, is specially bad for synchronization. In this case, there is a much stronger oscillation.

A. Critical values of ϵ

We have found out that, with all other parameters fixed, there is always a critical value of ϵ , which we call ϵ^* such that, if $\epsilon > \epsilon^*$ the system stays synchronized almost surely, meaning that among the $N_s = 1000$ samples launched, all of them stayed synchronized up to time 10^6 . Fig. 7 shows the critical ϵ^* for Bernoulli systems as a function of the network fluctuation time, using fixed values for the other parameters, $T_d = 100$ and $p = 1/2$. The three curves correspond to different system sizes $N = 20, 40$ and 80 .

Notice that, for $N = 40$ and $\epsilon = 0.7$ the transition curve presents a reentrant behavior: the critical curve is crossed three times (see dashed horizontal line in Fig. 7). This explains the peculiar behavior found in the synchronization level averages in Fig. 6.

But Fig. 7 (top) provides more information. In all cases, ϵ^* is minimal for small T_n . This implies that synchronization is most likely to happen for fast network fluctuations. Also, for very large T_n the values of ϵ^* tend to one: synchronization becomes nearly impossible. For network fluctuation times $T_n \sim T_d$ we have an interesting increase in the value of ϵ^* , thus implying that when *both time-scales collide, synchronizability is lower*. This phenomenon bears similarity to observations reported on neural network models with spike-timing dependent plasticity [37].

The bottom panel of Fig. 7 shows the same average (static) SLE as a function of ϵ and p for a Bernoulli system with $N = 40$ and $T_d = 100$, marking also in white the zero SLE line, i.e.: synchronization in average. The yellow line marks the critical ϵ^* line of almost-sure synchronization for $T_n = 10$, which is below the average synchronization line for static networks. This means that even values of the parameters which do not yield synchronization in average, will still synchronize almost surely when subject to fast fluctuations.

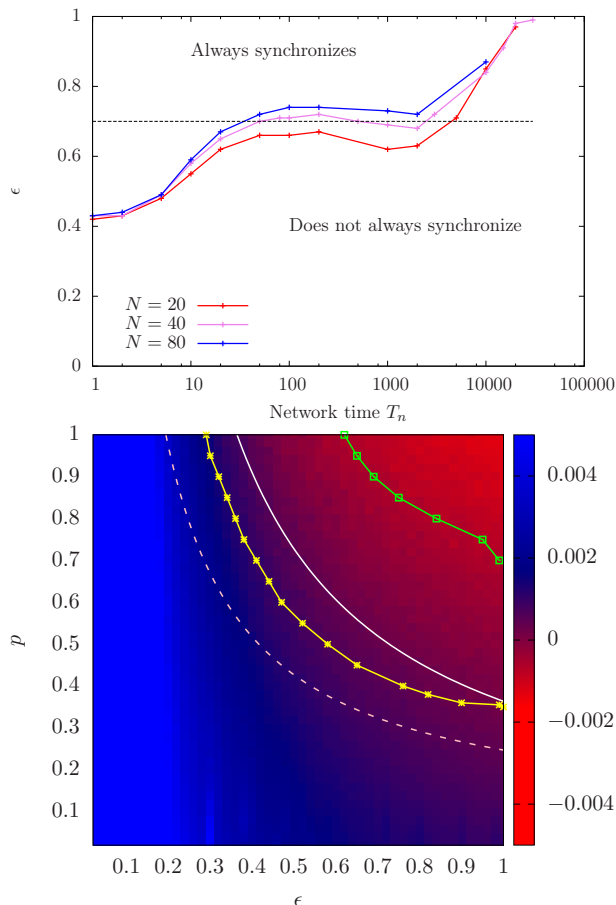


Figure 7: Top: Critical value ϵ^* as a function of T_n for different values of $N = 20, 40$ and 80 . In all cases, $T_d = 100$ and $p = 1/2$, and the dynamical system is Bernoulli. The horizontal dashed line corresponds to the results shown in Fig. 6 (center), $\epsilon = 0.7$. Bottom: same SLE plot as a function of ϵ and p as in Fig. 4, but adding extra lines. The yellow line denotes the ϵ^* values as a function of p for very fast fluctuations, $T_n = 10$. Notice that even systems with positive average SLE will synchronize for those fast fluctuations. For comparison, the green line denotes the ϵ^* value for very slow fluctuations, $T_n = 10^4$. The dashed pink line denotes the mean-field approximation given by Eq. (11). The continuous white line corresponds to the theoretical synchronization region of a static network, from Eq. 10 and is included for comparison with the non fluctuating case.

This enhancement of the synchronizability for rapidly fluctuating networks has also been observed in networks of oscillators with diffusive coupling [21, 26]. Moreover, the fast-switching approximation states that when the time-scale of the network fluctuations is much larger than the typical time-scale of the oscillator dynamics, the synchronization properties are well described by a mean-field network. This is not the case here: the pink dashed line in Fig. 7 (bottom) delimits the mean-field synchronization region expected from the spectrum in Eq. (11). As we can see, it departs from the yellow curve for fast network fluctuations, hence in our setting the mean-field

curve does not provide a good approximation for the synchronization region of the fast switching regime, marked by the yellow curve. Notice that our setting is different from the classic fast switching approximation framework, which was developed for diffusive coupling. Instead, our couplings are given by the stochastic adjacency matrix and not by the Laplacian. Also, our internal time-scale T_d is a time-delay which does not inform us of the necessary time to reach synchronization, which could be in fact infinite for a non-synchronizing configuration. Still, the behaviour is qualitatively similar and the synchronizability is enhanced for $T_n \ll T_d$.

Finally, the green line shows the ϵ^* line for $T_n = 10^4$. This corresponds to the static network regime $T_n \gg T_d$. The synchronization region is much smaller: for slow fluctuations, it is very difficult to force the system to synchronize.

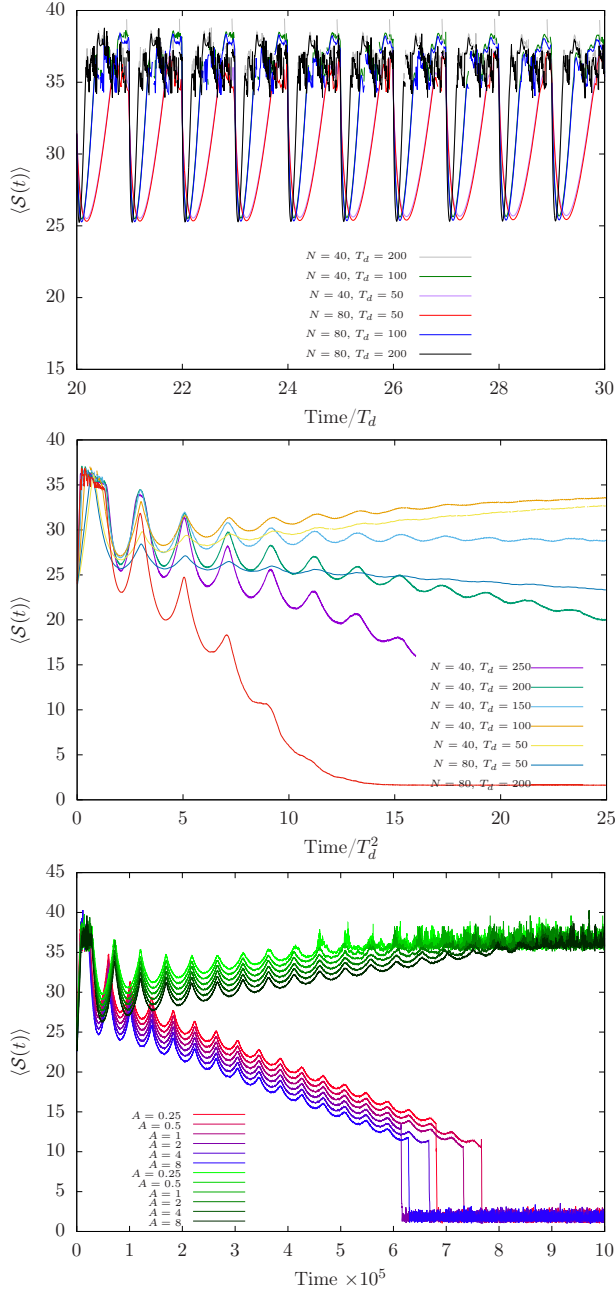
B. Synchronization oscillations

A very salient feature of the average synchronization level curves in Fig. 6 is the presence of oscillations, which decay with time. The oscillations all show a periodicity related to the time delay T_d , and they have the same phase for different values of the network switching time T_n . We illustrated this in further detail in Fig. 8 (top), which shows the average synchronization level for a short time-span for all time-steps (not only multiples of 100) using different values of N and T_d . These oscillations are independent of the network fluctuations, and they appear as well in fixed networks, as shown in Fig. 8 (bottom).

Upon this primary oscillation we have found a secondary oscillation, which periodicity scales with the square of the time-delay, T_d^2 . In Fig. 8 (center) we have removed the primary period, by showing only times multiple of T_d , and we represent a longer time span, with the time axis rescaled to t/T_d^2 . Again, these fluctuations have the same frequency and phase in all cases.

These oscillations are related to our choice of initial condition: we perturb the system at $t = 0$, and this perturbation decays initially. The initial decay is a typical behavior for weakly chaotic systems [28]. After a delay time the perturbation reappears, and this reappearance of a delay echo can be related to the observed periodicity equal to the delay time. For Bernoulli maps the evolution can even be calculated explicitly, we included the analytic calculations in appendix B.

This delay echo is transformed each time-delay interval and its shape gradually changes from an exponential decay to decaying oscillatory motion. This is illustrated in Fig. 9, where we show the analytically calculated evolution of a point-like perturbation along a specific direction in a fixed network of Bernoulli elements. While the initial perturbation (blue line) decays exponentially, the consecutive delay echoes are broader, and reach their maximal amplitude at a later point in time within the delay interval. However, the exact mathematical origin of the



checked numerically that conjecture and found it to be inaccurate. In Fig. 10 we consider SW networks with $N = 40$ and $p = 1/2$, on which we set up a Bernoulli interacting system with $T_d = 100$ and $\epsilon = 0.7$. The difference is that the network fluctuations are only allowed to explore the ensemble of *low gap* graphs. Specifically, we reject all SW networks whose gap is larger than $\Delta_* = 0.1$. Approximately, the probability of rejection with these parameters is $1/2$. Nonetheless, the probability of one of these networks to synchronize is negligible ($< 10^{-6}$ in our numerical experiments). Fig. 10 shows the average synchronization for 100 realizations, using $T_n = 10, 100$ and 1000 , and found that, for fast enough fluctuations, the system *synchronizes*. Again, the same oscillations can be seen. This last result is reminiscent of the *Parrondo games* [38], where the alternation of losing strategies can give rise to a winning one. A random alternation of non-synchronizing networks can result strongly synchronizing.

V. CONCLUSIONS AND FURTHER WORK

The possibility to enhance the stability of a system through fast oscillations or fluctuations is a topic of long tradition, e.g. the Kapitza pendulum [39]. In this work we have explored the effect of topology fluctuations on the synchronizability of small-world networks of time-delayed coupled chaotic maps. We have first studied synchronizability of static networks sampled from the Newman-Watts small world network ensemble with N nodes and a fraction p of shortcuts. The spectral gap was found to be approximately given by $p/4$ independently of N and it showed a clear relationship with the synchronization Lyapunov exponent for networks of Bernoulli and Logistic maps. The Bernoulli map case followed closely the theoretical prediction, while the mapping was more nonlinear for the Logistic maps.

We then studied how the synchronization properties are affected by a time varying coupling topology. We found the stability of the synchronized state to be strongly affected by the interplay between the time-scale of the delayed interactions, T_d , and that of the network fluctuations, T_n . For the fast-switching regime, $T_n \ll T_d$, we obtain a strong enhancement of the synchronizability of the network. Even when we restrict our topology fluctuations to only explore those networks which would not be able to synchronize under static conditions, we can obtain almost-sure synchronization under fast enough fluctuations. This result is in qualitative agreement with the fast switching approximation [26]. For $T_n \sim T_d$ we observe a severe reduction in synchronizability, which is recovered as we increase $T_n > T_d$. Nonetheless, for $T_n \gg T_d$ the system will nearly always desynchronize. Moreover, we observe oscillations in the synchronization level, when the network is close to the synchronized state. These oscillations have a periodicity related to T_d and are typical of the weak chaos regime. For our choice of

perturbation, these oscillations can be analytically recovered in a network of Bernoulli maps. We also report a secondary oscillation of periodicity scaling with T_d^2 .

We have restricted ourselves to the case of small-world networks, because they are more amenable to a mean-field approach, but it is relevant to ask whether these results also apply to other network ensembles, such as purely random Erdős-Rényi graphs or scale-free networks; as well as to other dynamical systems beyond Bernoulli or Logistic.

Acknowledgments

We would like to acknowledge W. Kinzel and A. Deaño. This work was partly supported by the Spanish Government through grant FIS-2012-38866-C05-1 (J.R.-L.) and the Alexander von Humboldt Foundation within the Renewed research stay program (E.K.).

Appendix A: Mean-field spectrum and eigengap of the SW networks

Our ensemble is composed of networks which consist of a directed ring of N nodes to which we add Np directed shortcuts. Here we compute the spectrum of the networks of this ensemble within the mean-field approximation of [32], in order to characterize the eigengap. The strategy is as follows: we obtain the ensemble average of each adjacency matrix entry, $\langle G_{ij} \rangle$, and study the spectrum of the resulting matrix, which will be a *circulant matrix*,

$$G^{\text{MF}} = \begin{bmatrix} c_0 & c_{N-1} & \dots & c_2 & c_1 \\ c_1 & c_0 & \dots & c_3 & c_2 \\ \vdots & \vdots & \ddots & \vdots & \vdots \\ c_{N-1} & c_{N-2} & \dots & c_1 & c_0 \end{bmatrix}, \quad (\text{A1})$$

whose eigenvalues can be computed analytically [27]:

$$\gamma_m^{\text{MF}} = \sum_k c_k \exp \left[\frac{-2\pi i m k}{N} \right], \quad (\text{A2})$$

where $m = 0, \dots, N-1$. Before the shortcuts are introduced, $c_1 = 1$ and all other entries $c_i = 0$, $i \neq 1$. When the shortcuts are introduced, the subdiagonal elements become $G_{i,i+1} = 1/(1+n_s)$, where n_s is the number of shortcuts reaching element i . Thus,

$$c_1 = \langle G_{i,i+1} \rangle = \left\langle \frac{1}{1+n_s} \right\rangle. \quad (\text{A3})$$

The random variable n_s follows a binomial distribution: each site can be reached by $\approx N$ possible shortcuts, each

of them with probability $\approx p/N$. Thus, its probability distribution is given by

$$P(n_s) \approx \binom{N}{n_s} \left(\frac{p}{N}\right)^{n_s} \left(1 - \frac{p}{N}\right)^{N-n_s}, \quad (\text{A4})$$

which, in the limit where $p/N \ll 1$ approaches the Poisson distribution

$$P(n_s) \approx e^{-p} \frac{p^{n_s}}{n_s!}. \quad (\text{A5})$$

For this distribution it is possible to obtain the desired expected value:

$$\begin{aligned} c_1 &= \left\langle \frac{1}{1+n_s} \right\rangle \approx \sum_{n_s=0}^{\infty} \frac{1}{1+n_s} e^{-p} \frac{p^{n_s}}{n_s!} \\ &= \frac{e^{-p}}{p} \sum_{x=1}^{\infty} \frac{p^x}{x!} \\ &= \frac{1 - e^{-p}}{p}, \end{aligned} \quad (\text{A6})$$

where we choose $x = n_s + 1$. The rest of the entries of the circulant matrix are all equal, $c_i = \tilde{c}$ for $i \neq 1$, and can be found by normalization:

$$\tilde{c} \approx \frac{1}{N-1} \left(1 - \frac{1 - e^{-p}}{p}\right). \quad (\text{A7})$$

Thus, applying (A2) we have

$$\gamma_m^{\text{MF}} = \tilde{c} + c_1 e^{\frac{2\pi i m}{N}} + \tilde{c} \sum_{k=2}^{N-1} e^{\frac{2\pi i k m}{N}}. \quad (\text{A8})$$

If $m = 0$, we obtain $\gamma_0 = 1$. The last term can be evaluated as a geometric sum or, alternatively, we can realize that if k was extended from 0 to $N-1$, it would yield zero. In both cases, we obtain

$$\gamma_m^{\text{MF}} = (c_1 - \tilde{c}) e^{-\frac{2\pi i m}{N}}. \quad (\text{A9})$$

Thus, the modulus of all eigenvalues for $m > 0$ is equal:

$$|\gamma_m^{\text{MF}}| \approx c_1 - \tilde{c} = \frac{1 - e^{-p}}{p} - \frac{1}{N-1} \left(1 - \frac{1 - e^{-p}}{p}\right). \quad (\text{A10})$$

Neglecting corrections of order N^{-1} , the eigenvalue gap is:

$$\Delta = 1 - \max \{|\gamma_{m \neq 0}^{\text{MF}}|\} \approx 1 - \frac{1 - e^{-p}}{p}. \quad (\text{A11})$$

Appendix B: Analytic explanation of the synchronization oscillations

We show in this appendix how synchronization oscillations arise generically, as the network decays towards or drifts away from the synchronization manifold. We consider a network of Bernoulli maps and the network structure to be fixed.

In this case, as the initial perturbation $\xi(\mathbf{t})$ is small, we linearize around the synchronization manifold $u_i(t) = \mu(t)$. The evolution of the network is then given by

$$\begin{aligned} \xi_i(t+1) &= (1 - \epsilon) f'(\mu(t)) \xi_i(t) + \\ &\quad \epsilon \sum_j G_{ij} f'(\mu(t - T_d)) \xi_j(t - T_d). \end{aligned} \quad (\text{B1})$$

After decomposition along the eigenvectors $\{v_k\}$ of G , we can rewrite Eq. (B1) as

$$\begin{aligned} v_k(t+1) &= (1 - \epsilon) f'(\mu(t)) v_k(t) + \\ &\quad \epsilon \gamma_k f'(\mu(t - T_d)) v_k(t - T_d), \end{aligned} \quad (\text{B2})$$

where γ_k denotes the eigenvalue of G along the eigenvector v_k . For Bernoulli maps, the derivative along the chaotic trajectory is constant, $f'(u(t)) = a$, we can simplify Eq. (B2) as

$$v_k(t+1) = (1 - \epsilon) a v_k(t) + \epsilon \gamma_k a v_k(t - T_d). \quad (\text{B3})$$

The exponential decay of a perturbation is slowest (or the growth is fastest) along the direction with the smallest eigenvalue gap $1 - |\gamma_2|$, we thus only consider the direction $v_2(t)$. To find the evolution along a direction v_k , one can simply replace γ_2 by γ_k in the calculations. In the simulations we applied a perturbation $\xi(t)$ only at $t = 0$, with a randomized magnitude over the network nodes. For simplicity, we will assume this magnitude along the direction $v_2(0) = 1$, while $v_2(t < 0) = 0$. We can then solve Eq. (B3) directly, and we find for the first delay interval, $0 \leq t < T_d$,

$$v_2(t+1) = (1 - \epsilon) a v_2(t), \quad (\text{B4})$$

which is solved by

$$v_2(t) = ((1 - \epsilon)a)^t \text{ for } 0 < t \leq T_d. \quad (\text{B5})$$

The perturbation initially evolves with a rate given by $\ln |(1 - \epsilon)a|$, which corresponds to the instantaneous Lyapunov exponent [7, 28]. We only consider networks in the weakly chaotic regime, meaning that the instantaneous Lyapunov exponent is negative and that the perturbation initially decays.

Using Eq. (B5) as initial function for the next delay interval $T_d \leq t < 2T_d + 1$, this leads to an equation of motion

$$v_2(t+1) = (1 - \epsilon) a v_2(t) + \epsilon a \gamma_2 ((1 - \epsilon)a)^t. \quad (\text{B6})$$

Imposing continuity, $v_2(T_d) = ((1 - \epsilon)a)^{T_d}$, this difference equation is solved by

$$v_2(t) = ((1 - \epsilon)a)^t + (t - T_d)\epsilon a \gamma_2 ((1 - \epsilon)a)^{t - T_d - 1}, \quad (\text{B7})$$

for $T_d < t \leq 2T_d + 1$. Hence, the initial perturbation reappears after a time $T_d + 1$, but the delay echo is broadened. In general, we find for $n(T_d + 1) \leq t < (n + 1)(T_d + 1)$

$$v_2(t) = \sum_{k=0}^n \frac{1}{k!} ((1 - \epsilon)a)^{t - kT_d - k} (a\epsilon\gamma_2)^k \prod_{l=0}^{k-1} (t - kT_d - l). \quad (\text{B8})$$

We find additional delay echoes appearing at multiples

of $T_d + 1$, each one broader than the previous. After several cycles the resulting motion indeed resembles an oscillation, with a periodicity approximated as

$$T \approx T_d + 1/2 - 1/\ln|a(1 - \epsilon)|,$$

in the limit of large delay $T_d \rightarrow \infty$. This is illustrated in Fig. 9. We remark here that in general, γ_2 is a complex number, which could lead to additional oscillations with a periodicity related to the delay time and the phase of γ_2 .

References

-
- [1] S. Boccaletti, J. Kurths, G. Osipov, D. Valladares, and C. Zhou, *Physics Reports* **366**, 1 (2002).
 - [2] L. M. Pecora and T. L. Carroll, *Phys. Rev. Lett.* **80**, 2109 (1998).
 - [3] V. Flunkert, S. Yanchuk, T. Dahms, and E. Schöll, *Phys. Rev. Lett.* **105**, 254101 (2010).
 - [4] F. M. Atay, J. Jost, and A. Wende, *Phys. Rev. Lett.* **92**, 144101 (2004).
 - [5] T. Heil, I. Fischer, W. Elsässer, J. Mulet, and C. Mirasso, *Phys. Rev. Lett.* **86**, 795 (2001).
 - [6] I. Fischer, R. Vicente, J. Buldu, M. Peil, C. Mirasso, M. Torrent, and J. Garcia-Ojalvo, *Phys. Rev. Lett.* **97**, 123902 (2006).
 - [7] S. Heiligenthal, T. Dahms, S. Yanchuk, T. Jüngling, V. Flunkert, I. Kanter, E. Schöll, and W. Kinzel, *Phys. Rev. Lett.* **107**, 234102 (2011).
 - [8] M. Nixon, M. Fridman, E. Ronen, A. A. Friesem, N. Davidson, and I. Kanter, *Phys. Rev. Lett.* **108**, 214101 (2012).
 - [9] A. Argyris, D. Syvridis, L. Larger, V. Annovazzi-Lodi, P. Colet, I. Fischer, J. García-Ojalvo, C. R. Mirasso, L. Pesquera, and K. A. Shore, *Nature* **438**, 343 (2005).
 - [10] I. Kanter, E. Kopelowitz, and W. Kinzel, *Phys. Rev. Lett.* **101**, 084102 (2008).
 - [11] G. Buzsaki, *Rhythms of the brain* (Oxford University Press, 2006).
 - [12] I. Kanter, E. Kopelowitz, R. Vardi, M. Zigzag, W. Kinzel, M. Abeles, and D. Cohen, *EPL (Europhysics Letters)* **93**, 66001 (2011).
 - [13] I. Kanter, M. Zigzag, A. Englert, F. Geissler, and W. Kinzel, *EPL (Europhysics Letters)* **93**, 60003 (2011).
 - [14] M. J. Martin, O. D’Huys, L. Lauerbach, E. Korutcheva, and W. Kinzel, *Phys. Rev. E* **93**, 022206 (2016).
 - [15] J. Feng, V. K. Jirsa, and M. Ding, *Chaos* **16**, 015109 (2006).
 - [16] P. Holme, *The European Physical Journal B* **88**, 1 (2015).
 - [17] D. V. Buonomano and M. M. Merzenich, *Annual Review of Neuroscience* **21**, 149 (1998), PMID: 9530495.
 - [18] I. V. Belykh, V. N. Belykh, and M. Hasler, *Physica D: Nonlinear Phenomena* **195**, 188 (2004).
 - [19] F. Peruani, E. M. Nicola, and L. G. Morelli, *New Journal of Physics* **12**, 093029 (2010).
 - [20] N. Fujiwara, J. Kurths, and A. Díaz-Guilera, *Phys. Rev. E* **83**, 025101 (2011).
 - [21] M. Frasca, A. Buscarino, A. Rizzo, L. Fortuna, and S. Boccaletti, *Phys. Rev. Lett.* **100**, 044102 (2008).
 - [22] N. Fujiwara, J. Kurths, and A. Díaz-Guilera, *Chaos* **26**, 094824 (2016).
 - [23] K. Uriu, S. Ares, A. C. Oates, and L. G. Morelli, *Phys. Rev. E* **87**, 032911 (2013).
 - [24] K. Uriu and L. G. Morelli, *Biophys J* **107**, 514 (2014).
 - [25] M. Nag and S. Poria, *Chaos, Solitons & Fractals* **91**, 9 (2016).
 - [26] D. J. Stilwell, E. M. Bollt, and D. G. Roberson, *SIAM Journal on Applied Dynamical Systems* **5**, 140 (2006).
 - [27] G. H. Golub and C. F. Van Loan, *Matrix Computations* (Johns Hopkins University Press, 1996).
 - [28] O. D’Huys, S. Zeeb, T. Jüngling, S. Yanchuk, and W. Kinzel, *EPL (Europhysics Letters)* **103**, 10013, (2013).
 - [29] T. Jüngling, O. D’Huys, and W. Kinzel, *Phys. Rev. E* **91**, 062918 (2015).
 - [30] M. Barahona and L. M. Pecora, *Phys. Rev. Lett.* **89**, 054101 (2002).
 - [31] Y. Aviad, I. Reidler, M. Zigzag, M. Rosenbluh, and I. Kanter, *Opt. Express* **20**, 4352 (2012).
 - [32] C. Grabow, S. Grosskinsky, J. Kurths, and M. Timme, *Phys. Rev. E* **91**, 052815 (2015).
 - [33] M. Newman and D. Watts, *Physics Letters A* **263**, 341 (1999).
 - [34] D. J. Watts and S. H. Strogatz, *Nature* **393**, 409 (1998).
 - [35] R. Kühn, *Journal of Physics A: Mathematical and Theoretical* **41**, 295002 (2008).
 - [36] J. Billen, M. Wilson, A. Baljon, and A. Rabinovitch, *Phys. Rev. E* **80**, 046116 (2009).
 - [37] A. Knoblauch, F. Hauser, M.-O. Gewaltig, E. Körner, and G. Palm, *Frontiers in computational neuroscience* **6**, 55 (2012).
 - [38] G. P. Harmer and D. Abbott, *Nature* **402**, 864 (1999).
 - [39] L. Landau and E. Lifshitz, *Mechanics* (Pergamon Press, 1960).
 - [40] S. N. Elaydi, *Discrete chaos: with applications in science and engineering* (CRC Press, 2007).
 - [41] The Lyapunov exponent of an isolated Bernoulli map

is $\lambda_B = \ln a \approx 0.09531$. The Lyapunov exponent of the Logistic map, λ_L , must be obtained computationally, but

a value of $r = 3.577$ gives $\lambda_B \approx \lambda_L$ [40].